

# Fluorescent 3-hydroxy-4-pyridinone hexadentate iron chelators: intracellular distribution and the relevance to antimycobacterial properties

Ana Nunes · Maria Podinovskaia · Andreia Leite ·  
Paula Gameiro · Tao Zhou · Yongmin Ma · Xiaole Kong ·  
Ulrich E. Schaible · Robert C. Hider · Maria Rangel

Received: 19 January 2010 / Accepted: 19 March 2010 / Published online: 3 April 2010  
© SBIC 2010

**Abstract** We report the synthesis and characterization of a fluorescent iron chelator (**4**), shown to be effective in inhibiting the growth of *Mycobacterium avium* in macrophages, together with the synthesis and characterization of two unsuccessful analogues selected to facilitate identification of the molecular properties responsible for the antimicrobial activity. Partition of the chelators in liposomes was investigated and the compounds were assessed

with respect to uptake by macrophages, responsiveness to iron overload/iron deprivation and intracellular distribution by flow cytometry and confocal microscopy. The synthesis of the hexadentate chelators is based on a tetrahedral structure to which three bidentate 3-hydroxy-4-pyridinone chelating units are linked via amide bonds. The structure is synthetically versatile, allowing further addition of functional groups such as fluorophores. Here, we analyse the non-functionalized hexadentate unit (**3**) and the corresponding rhodamine B (**4**) and fluorescein (**5**) labelled chelators. The iron(III) stability constant was determined for **3** and the values  $\log \beta = 34.4$  and  $\text{pFe}^{3+} = 29.8$  indicate an affinity for iron of the same order of magnitude as that of mycobacteria siderophores. Fluorescence properties in the presence of liposomes show that **4** strongly interacts with the lipid phase, whereas **5** does not. Such different behaviour may explain their distinct intracellular localization as revealed by confocal microscopy. The flow cytometry and confocal microscopy studies indicate that **4** is readily engulfed by macrophages and targeted to cytosol and vesicles of the endolysosomal continuum, whereas **5** is differentially distributed and only partially colocalizes with **4** after prolonged incubation. Differential distribution of the compounds is likely to account for their different efficacy against mycobacteria.

A. Nunes and M. Podinovskaia contributed equally to the manuscript.

**Electronic supplementary material** The online version of this article (doi:10.1007/s00775-010-0650-1) contains supplementary material, which is available to authorized users.

A. Nunes · A. Leite · P. Gameiro  
REQUIMTE, Departamento de Química, Faculdade de Ciências,  
Universidade do Porto, 4069-007 Porto, Portugal

M. Podinovskaia · U. E. Schaible  
Department of Infectious and Tropical Diseases,  
London School of Hygiene and Tropical Medicine,  
Keppel Street, London WC1E 7HT, UK

T. Zhou · Y. Ma · X. Kong · R. C. Hider  
Division of Pharmaceutical Sciences, King's College London,  
Franklin-Wilkins Building, London SE1 9NH, UK

T. Zhou  
College of Food and Biotechnology,  
Zhejiang Gongshang University,  
Hangzhou 310035, People's Republic of China

U. E. Schaible  
Department of Molecular Infection Biology,  
Research Center Borstel, 23845 Borstel, Germany

M. Rangel (✉)  
REQUIMTE, Instituto de Ciências Biomédicas de Abel Salazar,  
Universidade do Porto, 4099-003 Porto, Portugal  
e-mail: mcrangel@fc.up.pt

**Keywords** Fluorescent hexadentate iron(III) chelators ·  
Synthesis · Affinity constants · Partition in liposomes ·  
Confocal microscopy

## Introduction

Iron is an essential micronutrient for pathogenic bacteria as well as for the host organisms, thereby causing a competitive

relationship between host and pathogen [1–5]. To acquire iron from their environment, microbes have developed high-affinity iron-scavenging molecules, known as siderophores, which are hexadentate chelators that strongly complex iron and efficiently deliver the element inside the pathogen. Host defence strategies depend on iron for the generation of reactive oxygen and nitrogen intermediates. Iron distribution in the host is tightly controlled and iron sequestration by binding proteins such as lactoferrin and inflammation-triggered iron redistribution, as controlled by hepcidin, contribute to antimicrobial host defence. Consequently, pharmacological intervention by iron chelators has been considered as a therapy against bacterial infections [6–10]. The design of iron chelators capable of competing for iron with bacterial siderophores and which possess the required features to target infection sites will undoubtedly contribute to the implementation of novel therapeutic strategies.

In the particular case of mycobacteria, it is well known that these pathogens synthesize two types of siderophores: (1) mycobactins, which remain cell-wall-associated, and (2) carboxymycobactins and exochelins, which are released to the extracellular medium [15, 16]. These molecules have chelating units based on the phenyloxazolidine ring, ornithine-derived hydroxamates and salicylates. In the case of *Mycobacterium avium*, mycobactins and carboxymycobactins possess identical iron(III) binding sites and differ only in side chain characteristics, such that a lipophilic character is conferred on mycobactins and a hydrophilic character on carboxymycobactins [2, 4]. With this knowledge, we designed chelators based on 3-hydroxy-4-pyridinone ligands, which are known for their use in the treatment of iron-overloaded patients and which exhibit higher affinity for iron when compared with hydroxamates. The results from a systematic investigation centred on 15 iron chelators indicate that the 3-hydroxy-4-pyridinone hexadentate chelator (**4**), Fig. 1, is effective at inhibiting the growth of *M. avium*, an opportunistic pathogen able to survive in macrophages [11]. The data demonstrate that the antimicrobial activity is associated with the chelating properties of **4** and its ability to penetrate cell membranes to access the bacteria. Closely related compounds, with an identical affinity for iron, although exhibiting a positive response on the inhibition of bacterial growth in axenic media, were found not to be effective in the *M. avium* model [11].

Compound **4**, which results from the coupling of a hexadentate chelating unit and rhodamine B, appears to possess key molecular features that allow penetration through cell membranes. Rhodamine B conjugated peptides have previously been shown to have antimicrobial activity, the process being related to their surface activities mainly associated with the lipophilic rhodamine B residue

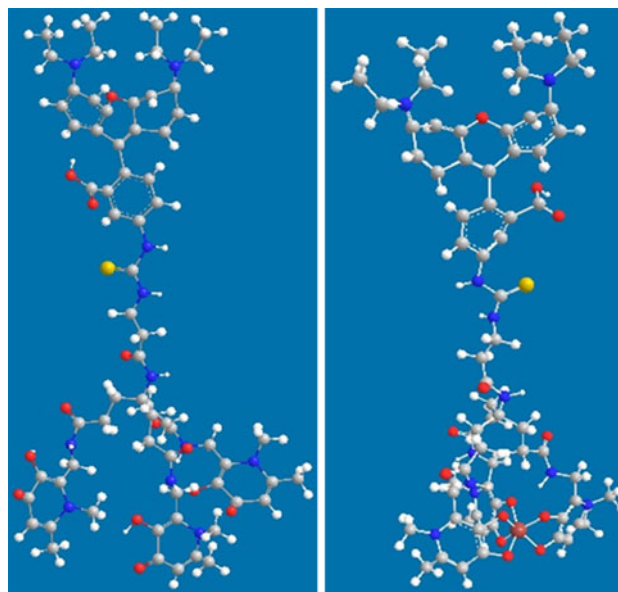


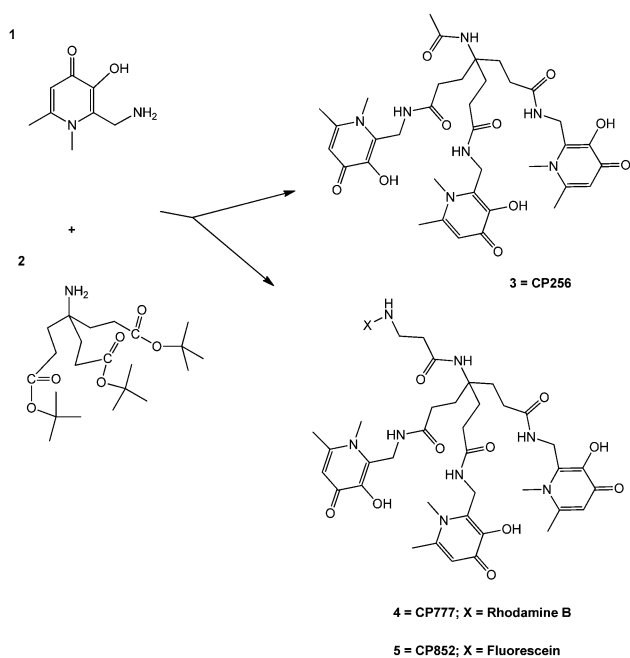
**Fig. 1** Structure of hexadentate chelator **4** and its iron(III) complex

[12]. Thus, the complete understanding of the iron acquisition pathways of bacteria will facilitate the identification of the optimal physicochemical properties for effective antimicrobial drugs. Several studies on structure and transport properties of amphiphilic siderophores such as acinetoferrin indicate that their hydrophilic/lipophilic properties are critical for their membrane permeation. Also, it has been proposed that the hydrophobic components of amphiphilic siderophores facilitate flip–flop diffusion through lipid membranes [13–16]. Mycobacteria scavenge extracellular iron from host proteins using hydrophilic siderophores such as carboxymycobactins [3, 5] and extraction of intracellular iron from macrophages is achieved by lipophilic mycobactins, the resulting mycobactin–iron complex accumulating in macrophage lipid droplets. It is thus clear that iron acquisition represents a realistic target for the control of mycobacterial infection [17].

In the present work we report the synthesis and properties of the rhodamine B derived chelator (**4**) and its fluorescein analogue (**5**). In an attempt to begin to understand the mode of action of **4**, we have investigated the distribution of the fluorescent chelators in both liposomes and macrophages.

## Materials and methods

For all the reactions, chemicals were obtained from Sigma–Aldrich (grade puriss, p.a.) and were used as received unless otherwise specified.



**Scheme 1** Formulae and numbering of hexadentate chelators and their precursors. Compounds **3**, **4** and **5** were designated as CP256, CP777 and CP852 in the study regarding the evaluation of their antimicrobial properties [11]

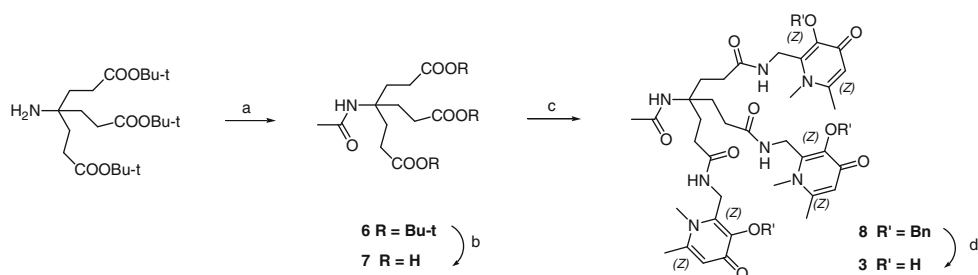
### Synthesis of hexadentate chelators

The synthesis of the 3-hydroxy-4-pyridinone hexadentate chelators is based on the coupling of three bidentate 3-hydroxy-4-pyridinone moieties (**1**) to a tripodal anchor (**2**) as outlined in Scheme 1.

### Tripodal hydroxypyridinone

The synthesis of tripodal hydroxypyridinone (**3**) is outlined in Scheme 2. The 2-aminomethyl-3-benzyloxy-1,6-dimethyl-1*H*-pyridin-4-one (**1**) was synthesized as previously described [18, 19]. The anchor molecule (**2**) was synthesized by a method described by Newkome et al. [20] starting from nitromethane and *tert*-butyl acrylate. The

**Scheme 2** Synthesis of **3**.  
*HOBt* *N*-hydroxybenzotriazole,  
*DCCI* dicyclohexylcarbodiimide,  
*DMF* dimethylformamide



**(a)** acetyl chloride, Et<sub>3</sub>N, CH<sub>2</sub>Cl<sub>2</sub>; **(b)** HCOOH; **(c)** HOBt, DCCI, 1,6-dimethyl-2-aminomethyl-3-benzyloxy-pyridin-4(1*H*)-one, DMF; **(d)** BCl<sub>3</sub>, CH<sub>2</sub>Cl<sub>2</sub>.

tripod possesses a free nitro group which can be reduced with freshly prepared Raney nickel to produce the corresponding primary amine (**2**). The starting anchor was acylated with acetyl chloride to produce di-*tert*-butyl 4-acetamido-4-(3-*tert*-butoxy-3-oxopropyl)heptanedioate (**6**). The three protecting *tert*-butyl groups of the resulting compound were removed using formic acid, producing 4-acetamido-4-(2-carboxyethyl)heptanedioic acid (**7**). Compound **1** was linked to the anchor structure by coupling the free amino group of the pyridinone to the acid groups of the anchor to give **8**, followed by deprotection with BCl<sub>3</sub> to yield the hexadentate chelator **3**.

### Di-*tert*-butyl 4-acetamido-4-(3-*tert*-butoxy-3-oxopropyl)heptanedioate

To a stirred solution of amine **2** (12 mmol) and triethylamine (12 mmol) in dichloromethane (40 mL), cooled with an ice-bath, acetyl chloride (10 mmol) was added. Stirring was continued overnight. The reaction mixture was washed successively with aqueous hydrochloric acid, aqueous sodium hydrogen carbonate and water, dried over Na<sub>2</sub>SO<sub>4</sub> and concentrated. The residue was subjected to column chromatography on silica gel (EtOAc/hexane) to give **6** (71%) as a white solid. m.p. 118–120 °C, <sup>1</sup>H NMR (360 MHz, CDCl<sub>3</sub>) δ: 1.44 (s, CH<sub>3</sub>, 27H), 1.92 (s, CH<sub>3</sub>, 3H), 1.97 (m, CH<sub>2</sub>, 6H), 2.23 (m, CH<sub>2</sub>, 6H), 5.92 (s, NH, 1H). <sup>13</sup>C NMR (90 MHz, dimethyl-*d*<sub>6</sub> sulfoxide, DMSO-*d*<sub>6</sub>) δ: 24.3 (CH<sub>3</sub>CO), 28.1 (CH<sub>3</sub>), 29.8 (CCH<sub>2</sub>CH<sub>2</sub>), 30.0 (CCH<sub>2</sub>CH<sub>2</sub>), 57.4 (NHC), 80.7 (OCMe<sub>3</sub>), 169.6 (CH<sub>3</sub>CO), 172.9 (COOBu-*t*). Electrospray ionization (ESI) mass spectrometry (MS): *m/z* 458.17 ([M+H]<sup>+</sup>).

### 4-Acetamido-4-(2-carboxyethyl)heptanedioic acid

A solution of *tert*-butyl ester **6** (10 mmol) in formic acid (96%, 10 mL) was stirred at 25 °C overnight. After concentration, toluene (5 mL) was added and the solution was again evaporated in a vacuum to remove azeotropically any residual formic acid. The residue was then precipitated in

acetone (50 mL) to afford 4-acetamido-4-(2-carboxyethyl)heptanedioic acid (**7**; 95%) as a yellow solid, which could be used for the next step without further purification. m.p. 124–126 °C,  $^1\text{H}$  NMR (360 MHz, DMSO- $d_6$ )  $\delta$ : 1.78 (s, CH<sub>3</sub>, 3H), 1.81 (m, CH<sub>2</sub>, 6H), 2.10 (m, CH<sub>2</sub>, 6H), 7.19 (s, NH, 1H).  $^{13}\text{C}$  NMR (90 MHz, DMSO- $d_6$ )  $\delta$ : 23.8 (CH<sub>3</sub>), 28.4 (CCH<sub>2</sub>CH<sub>2</sub>), 29.3 (CCH<sub>2</sub>CH<sub>2</sub>), 56.7 (NHC), 169.5 (CH<sub>3</sub>CO), 174.8 (COOH). ESI-MS:  $m/z$  290.12 ([M+H]<sup>+</sup>).

#### Protected hexadentate ligand

A mixture of triacid **7** (0.867 g, 3 mmol), 1,6-dimethyl-2-aminomethyl-3-benzyloxy-pyridin-4(1H)-one (2.79 g, 10.8 mmol), dicyclohexylcarbodiimide (DCCl; 2.22 g, 10.8 mmol), *N*-hydroxybenzotriazole (HOBT; 1.46 g, 10.8 mmol) and dimethylformamide (DMF; 30 mL) was stirred for 2 days. After filtration and removal of solvent under reduced pressure, the residue was chromatographed in a silica gel column using methanol/chloroform (1:4) as an eluent to afford protected hexadentate ligand **8** (2.23 g, 73% yield) as a white solid.  $^1\text{H}$  NMR (360 MHz, DMSO- $d_6$ )  $\delta$ : 1.74 (s, CH<sub>3</sub>, 3H), 1.79 (m, CH<sub>2</sub>, 6H), 2.03 (m, CH<sub>2</sub>, 6H), 2.25 (s, CH<sub>3</sub>, 9H), 3.39 (s, CH<sub>3</sub>, 9H), 4.33 (d,  $J = 4.8$  Hz, 6H), 5.06 (s, CH<sub>2</sub>, 6H), 6.18 (s, pyridinone C5-H, 3H), 7.19 (s, NH, 1H), 7.35 (m, ArH, 9H), 7.41 (m, ArH, 6H), 8.09 (t,  $J = 4.8$  Hz, NH, 3H).  $^{13}\text{C}$  NMR (90 MHz, DMSO- $d_6$ )  $\delta$ : 20.4 (CH<sub>3</sub>), 23.9 (CH<sub>3</sub>CO), 29.7 (CCH<sub>2</sub>CH<sub>2</sub>), 30.3 (CCH<sub>2</sub>CH<sub>2</sub>), 34.8 (NHCH<sub>2</sub>), 36.0 (NCH<sub>3</sub>), 57.0 (NHC), 72.5 (PhCH<sub>2</sub>O), 117.8 (C-5H in pyridinone), 128.2 (CH in Ar), 128.6 (CH in Ar), 128.8 (CH in Ar), 138.0 (C in Ar), 140.6 (C-2 in pyridinone), 146.0 (C-3 in pyridinone), 148.1 (C-6 in pyridinone), 169.2 (CH<sub>3</sub>CO), 172.4 (CO), 172.5 (C-4 in pyridinone). MS: calculated for C<sub>57</sub>H<sub>68</sub>N<sub>7</sub>O<sub>10</sub>: 1,010.5027 (monoisotopic molecular weight M+H), found: ESI-MS: 1,010.5 [M+H]<sup>+</sup>, 505.8 [M+2H]<sup>2+</sup>; high-resolution MS-ESI: 1,010.5020 [M+H]<sup>+</sup>.

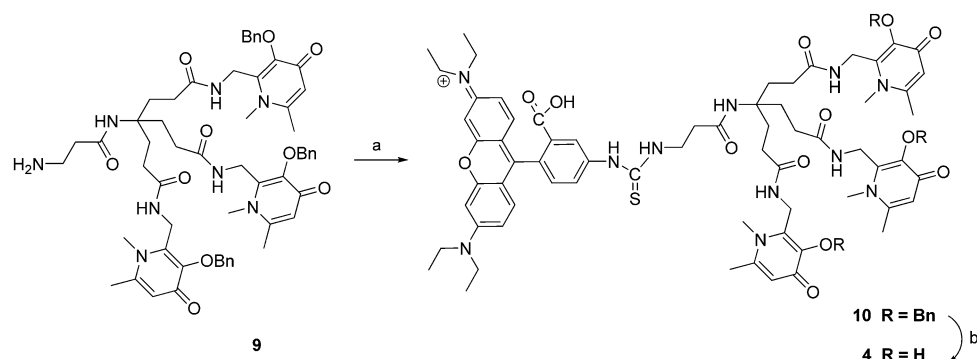
#### Hexadentate chelator 3 hydrochloride

De-benzylation of **8** was achieved by hydrogenation at 30 psi H<sub>2</sub> in the presence of 5% Pd/C (10% w/w of **8**) in ethanol for 6 h. The catalyst was removed by filtration and the combined filtrates were acidified to pH 1 with concentrated hydrochloric acid. After the solvents had been removed to dryness, the residues were purified by recrystallization from methanol/acetone to give hexadentate chelator **3** hydrochloride (92%) as a white powder.  $^1\text{H}$  NMR (360 MHz, DMSO- $d_6$ )  $\delta$ : 1.76 (s, CH<sub>3</sub>, 3H), 1.79 (m, CH<sub>2</sub>, 6H), 2.08 (m, CH<sub>2</sub>, 6H), 2.57 (s, CH<sub>3</sub>, 9H), 3.88 (s, CH<sub>3</sub>, 9H), 4.56 (d,  $J = 5.0$  Hz, 6H), 7.28 (s, NH, 1H), 7.29 (s, pyridinone C5-H, 3H), 8.93 (t,  $J = 5.0$  Hz, NH, 3H).  $^{13}\text{C}$  NMR (360 MHz, DMSO- $d_6$ )  $\delta$ : 21.0 (CH<sub>3</sub>), 23.8 (CH<sub>3</sub>CO), 29.6 (CCH<sub>2</sub>CH<sub>2</sub>), 30.3 (CCH<sub>2</sub>CH<sub>2</sub>), 35.1 (NHCH<sub>2</sub>), 39.5 (NCH<sub>3</sub>), 57.0 (NHC), 113.1 (C-5H in pyridinone), 140.3 (C-2 in pyridinone), 143.0 (C-3 in pyridinone), 148.9 (C-6 in pyridinone), 159.9 (C-4 in pyridinone), 169.3 (CH<sub>3</sub>CO), 173.8 (CONH). MS: calculated for C<sub>36</sub>H<sub>50</sub>N<sub>7</sub>O<sub>10</sub>: 740.3618 (monoisotopic molecular weight M+H), found: matrix-assisted laser desorption/ionization time of flight MS: 740.4 [M+H]<sup>+</sup> ( $\alpha$ -cyano-4-hydroxycinnamic acid as the matrix); high-resolution MS-ESI: 740.3621[M+H]<sup>+</sup>. Elemental analysis for (C<sub>36</sub>H<sub>48</sub>N<sub>7</sub>O<sub>14</sub>·3HCl·6H<sub>2</sub>O). Calculated (found): C 47.55 (46.93); H 6.49 (6.56); N 10.49 (10.64).

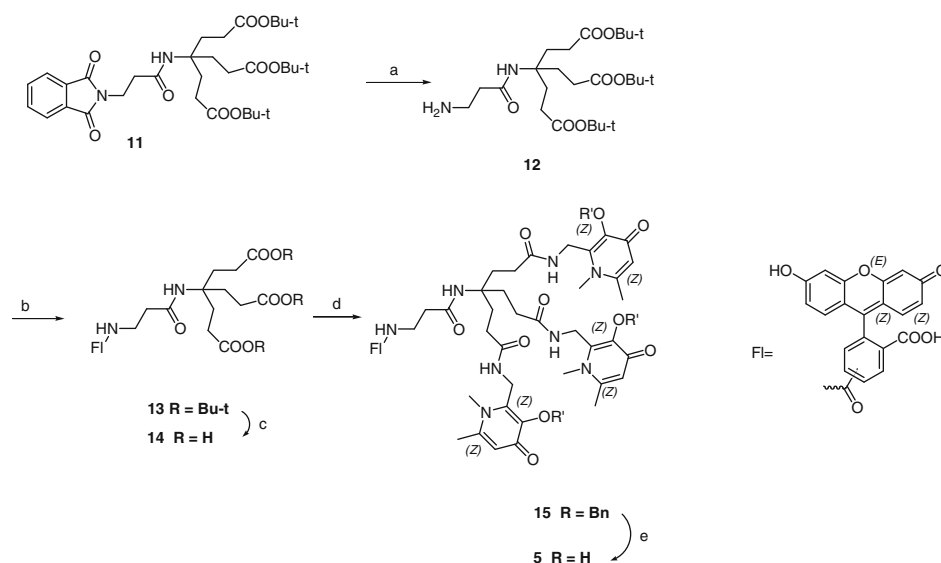
#### Rhodamine-labelled tripodal hydroxypyridinone

The synthesis of the rhodamine-labelled hexadentate compound is outlined in Scheme 3. The starting molecule **9** was obtained by hydrazinolysis of the amino group of the corresponding phthalimido tripodal precursor [21]. Compound **9** was coupled with rhodamine B isothiocyanate in the presence of anhydrous DMF and triethylamine to produce **10**, followed by deprotection with BCl<sub>3</sub> to yield rhodamine-labelled tripodal hydroxypyridinone (**4**).

**Scheme 3** Synthesis of **4**



(a) DMF, Et<sub>3</sub>N; (b) BCl<sub>3</sub>, CH<sub>2</sub>Cl<sub>2</sub>.

**Scheme 4** Synthesis of **5**. *NHS* *N*-hydroxysuccinimide

(a)  $\text{NH}_2\text{NH}_2$ , EtOH; (b) HOBt, DCCI, 5(6)-carboxy-fluorescein (c) HCOOH, (d) DCCI, NHS, 1,6-dimethyl-2-aminomethyl-3-benzyloxy-pyridin-4(1H)-one, DMF; (e)  $\text{BCl}_3$ ,  $\text{CH}_2\text{Cl}_2$ .

### Compound 10

To a solution of 100 mg of rhodamine B isothiocyanate (1.87 mmol) in anhydrous DMF (20 mL), 26  $\mu\text{L}$  (1.87 mmol) of triethylamine and 290 mg (2.8 mmol) of **9** were added and the mixture was stirred at room temperature overnight. The product was purified by gradient column chromatography, eluting with methanol/chloroform (1:1) and ammonia to afford **10** (4%) as a purple solid.  $^1\text{H}$  NMR (360 MHz,  $\text{CDCl}_3$ )  $\delta$ : 1.26 (t, 12H,  $\text{CH}_3$ ); 1.96 (d, 6H,  $\text{CH}_2$ ); 2.17 (d, 6H,  $\text{CH}_2$ ); 2.31 (s, 9H,  $\text{CH}_3$ ); 2.58 (s, 2H,  $\text{CH}_2$ ); 3.32 (q, 8H,  $\text{CH}_2$ ); (s, 9H,  $\text{CH}_3$ ); 3.67 (s, 9H,  $\text{CH}_3$ ); 3.38 (t, 2H,  $\text{CH}_2$ ); 4.40 (t, 6H,  $\text{CH}_2\text{N}$ ); 5.12 (d, 6H,  $\text{CH}_2\text{Ar}$ ); 6.47 (s, 3H,  $\text{H}_5$ ); 6.87–6.96 (m, 4H, Ar); 7.17 (d, 2H, Ar); 7.3–7.4 (m, 5H, Ar); 7.57 (d, 1H, Ar); 7.93 (d, 2H, Ar).

### Compound 4

Compound **10** (23 mg, 0.027 mmol) was dissolved in anhydrous dichloromethane (50 mL), under argon and cooled to 0  $^\circ\text{C}$ .  $\text{BCl}_3$  1 mL (0.0241 mmol) was added dropwise and the reaction mixture was kept overnight with stirring at room temperature. Methanol (50 mL) was added and the mixture was stirred for 1 h. The solid product that formed was removed by filtration and the solvent was removed under reduced pressure to afford the crude product. Recrystallization of the crude product from methanol/acetone (4:6) afforded **4** (36%) as a crystalline purple solid.  $^1\text{H}$  NMR (360 MHz,  $\text{DMSO}-d_6$ )  $\delta$ : 1.32 (t, 12H,  $\text{CH}_3$ );

2.00 (d, 6H,  $\text{CH}_2$ ); 2.27 (d, 6H,  $\text{CH}_2$ ); 2.64 (s, 9H,  $\text{CH}_3$ ); 3.32 (d, 2H,  $\text{CH}_2$ ); 3.68 (q, 8H,  $\text{CH}_2$ ); 3.99 (s, 9H,  $\text{CH}_3$ ); 3.99 (t, 2H,  $\text{CH}_2$ ); 4.64 (t, 6H,  $\text{CH}_2\text{N}$ ); 6.86 (s, 3H,  $\text{H}_5$ ); 6.97 (m, 4H, Ar); 7.06 (d, 2H, Ar); 7.25 (d, 1H, Ar); 7.26 (d, 2H, Ar).  $^{13}\text{C}$  NMR (90 MHz,  $\text{DMSO}-d_6$ )  $\delta$ : 21.0 ( $\text{CH}_3$ ), 23.8 ( $\text{CH}_3\text{CO}$ ); 29.6 ( $\text{CCH}_2\text{CH}_2$ ), 30.3 ( $\text{CCH}_2\text{CH}_2$ ), 35.1 ( $\text{NHCH}_2$ ), 39.5 ( $\text{NCH}_3$ ), 57.0 ( $\text{NHC}$ ), 113.1 ( $\text{C}-5$  in pyridinone), 140.3 ( $\text{C}-2$  in pyridinone), 143.0 ( $\text{C}-3$  in pyridinone), 148.9 ( $\text{C}-6$  in pyridinone), 159.9 ( $\text{C}-4$  in pyridinone), 169.3 ( $\text{CH}_3\text{CO}$ ), 173.8 ( $\text{CONH}$ ). MS: calculated for  $\text{C}_{66}\text{H}_{83}\text{N}_{11}\text{O}_{13}$  MS: 1269.6: (monoisotopic molecular weight  $\text{M}+\text{H}$ ), found: matrix-assisted laser desorption/ionization time of flight MS: 1269.6  $[\text{M}+\text{H}]^+$ . Elemental analysis for ( $\text{C}_{66}\text{H}_{83}\text{N}_{11}\text{O}_{13}\cdot 4\text{HCl}\cdot 6\text{H}_2\text{O}$ ). Calculated (found): C 50.12 (50.46); H 8.56 (8.63); N 5.74 (5.82).

### Fluorescein-labelled tripodal hydroxypyridinone

The synthesis of fluorescein-labelled tripodal hydroxypyridinone (**5**) is outlined in Scheme 4. The phthalimido tripodal ester (**11**) was prepared as described by Zhou et al. [21]. Deprotection of the amino group by hydrazinolysis yielded the amine (**12**), which was coupled with 5(6)-carboxyfluorescein in the presence of DCCI/HOBt to produce the triester (**13**). Compound **13** was hydrolysed by formic acid to generate the triacid **14**, which was coupled with 2-aminomethyl-3-benzyloxy-1,6-dimethyl-1*H*-pyridin-4-one to yield **15**, followed by deprotection with  $\text{BCl}_3$  to yield the hexadentate chelator **5**.

### Compound 12

To a solution of **11** (3 mmol) in ethanol (40 mL) was added 5.5% aqueous hydrazine (3 mL). After it had been refluxed for 3 h, the reaction mixture was cooled to 0 °C, acidified to pH 1 with concentrated hydrochloric acid and filtered. The filtrate was concentrated in a vacuum, and the residue was dissolved in distilled water (40 mL), adjusted to pH 12 with 10 mol NaOH and extracted with chloroform (5 × 100 mL). The combined organic extracts were dried over anhydrous Na<sub>2</sub>SO<sub>4</sub> under reduced pressure to furnish **12** (85%) as a pale-brown oil. <sup>1</sup>H NMR (CDCl<sub>3</sub>) δ: 1.43 (s, 27H), 1.94–1.99 (m, 6H), 2.19–2.24 (m, 6H), 2.29 (t, *J* = 5.9 Hz, 2H), 2.45 (br s, 2H), 3.00 (t, *J* = 5.9 Hz, 2H), 7.34 (br s, 1H).

### Compound 13

A mixture of **12** (5 mmol), 5(6)-carboxyfluorescein (5 mmol), DCCI (6 mmol) and HOBt (5.5 mmol) in DMF (50 mL) was stirred at room temperature for 1 day. After filtration, the solvent was removed under reduced pressure, and the residue was purified on a silica gel column using methanol/chloroform (1:9) as an eluent to afford **13** (59%) as a yellow foam. <sup>1</sup>H NMR (CDCl<sub>3</sub>) δ: 1.39 and 1.40 (2 s, 27H), 1.88–1.99 (m, 6H), 2.14–2.25 (m, 6H), 2.39 and 2.51 (2 m, *J* = 7.5 Hz, 2H), 3.59 and 3.70 (2 m, *J* = 7.5 Hz, 2H), 6.51–8.43 (m, 9H).

### Compound 14

A solution of *tert*-butyl ester **13** (10 mmol) in formic acid (96%, 10 mL) was stirred at 25 °C overnight. After concentration, toluene (5 mL) was added and the solution was again evaporated in a vacuum to remove azeotropically any residual formic acid. The residue was then precipitated in acetone (50 mL) to afford **14** (95%) as a yellow solid, which could be used for the next step without further purification. m.p. 189–201 °C. <sup>1</sup>H NMR (DMSO-*d*<sub>6</sub>) δ: 1.76–1.85 (m, 6H), 2.03–2.12 (m, 6H), 2.33 and 2.42 (2t, *J* = 6.9 and 7.1 Hz, 2H), 3.30–3.50 (m, 2H), 6.53–6.69 (m, 6H), 7.23–8.88 (m, 6H), 10.20 (brs, 1H).

### Compound 15

To a solution of **14** (10 mmol) in dry DMF (100 mL), DCCI (12 mmol) and *N*-hydroxysuccinimide (12 mmol) were added. The mixture was stirred for 2 h before 2-amino-methyl-3-benzyloxy-1,6-dimethyl-1*H*-pyridin-4-one (10 mmol) was added, and the reaction mixture was stirred at room temperature overnight. The precipitate was removed by filtration, and the solvent was evaporated. The residue was dissolved in dichloromethane and washed three times with 0.1 N NaOH and brine, dried over anhydrous Na<sub>2</sub>SO<sub>4</sub> and

concentrated under reduced pressure. The residue obtained was purified by column chromatography (methanol/chloroform, 1:9), affording **15** (54%) as a yellow solid. m.p. 195–216 °C. <sup>1</sup>H NMR (DMSO-*d*<sub>6</sub>) δ: 1.79 (m, 6H), 2.02 (m, 6H), 2.24 (s, 9H), 2.38 (m, 2H), 3.38 and 3.39 (2 s, 9H), 3.45 (m, 2H), 4.32 (s, 6H), 5.06 (s, 6H), 6.18 (s, 3H), 6.42–6.60 (m, 6H), 7.23–8.85 (m, 21H). *m/z* 1,397 [(M+1)]<sup>+</sup>.

### Compound 5

A solution of **15** (3 mmol) in dichloromethane (50 mL) was flushed with nitrogen. After the flask had been cooled to 0 °C, BCl<sub>3</sub> (1 mol in dichloromethane, 20 mL) was added dropwise and the reaction mixture was stirred at room temperature for 1 day. The excess BCl<sub>3</sub> was eliminated at the end of the reaction by the addition of methanol (10 mL) and the mixture was stirred for another 10 min. After removal of the solvents under reduced pressure, the residue was purified by recrystallization from methanol/acetone to afford **5** (40%) as a yellow solid. m.p. 198–213 °C. <sup>1</sup>H NMR (DMSO-*d*<sub>6</sub>) 1.81 (m, 6H), 2.09 (m, 6H), 2.40 (m, 2H), 2.56 (s, 9H), 3.34 (m, 2H), 3.87 and 3.88 (2 s, 9H), 4.55 (s, 6H), 6.56–8.93 (m, 12H), 10.25 (brs, 1H), 10.81 (brs, 1H). *m/z* 1,127 (M+1)<sup>+</sup>. Elemental analysis for (C<sub>58</sub>H<sub>62</sub>N<sub>8</sub>O<sub>16</sub>·3HCl·H<sub>2</sub>O·CHCl<sub>3</sub>). Calculated (found): C 51.58 (51.59); H 4.99 (5.23); N 8.16 (8.31).

### Determination of p*K*<sub>a</sub> and log β values

All solutions were prepared with double-deionized water (conductivity less than 0.1 μS cm<sup>-1</sup>). Solutions of NaOH were prepared in deionized water previously purged with argon while boiling to reduce carbonate impurity by dilution of a saturated stock solution. Hydrochloric acid (1 mM) solution was prepared by dilution of standard solution of hydrochloric acid (Tritisol). Hydrochloric acid (Tritisol) and all other chemicals were purchased from Merck (pro analysis grade).

All potentiometric measurements were carried out with a Crison 2002 pH meter and a Crison 2031 burette controlled by a computer. The electrode assembly consisted of an Orion 900029 double-junction AgCl/Ag reference electrode and a Russell SWL07 glass electrode. System calibration was performed by the Gran method [22] in terms of hydrogen ion concentration, by titrating solutions of strong acid with strong base. A calibration was performed before each run. All titrations were carried out under an argon atmosphere in a thermostat-controlled double-walled glass cell; the temperature was maintained at 25.0 ± 0.1 °C, and the ionic strength was adjusted to 0.10 M with sodium chloride.

The dissociation constants of **3** were obtained by titration of 20 mL of an acidified aqueous solution of the

compound (1 mM; 1.5 mM HCl), with approximately 0.03 mol NaOH, under an argon atmosphere. The values of the equilibrium constants defined by Eq. 1 were refined by least-squares calculation using the computer program Hyperquad [23].

#### Spectrophotometric measurements

Absorption spectra were recorded with a UNICAM UV-300 spectrophotometer equipped with a constant-temperature cell holder. Spectra were recorded at 25.0 °C in 1-cm quartz cuvettes with a slit width of 2 nm in the range 230–400 nm. Typical solution concentrations were 0.1 mol NaCl, 1 mmol ligand, 1 mmol *N,N'*-bis(2-hydroxybenzyl)ethylenediamine-*N,N'*-diacetic acid) (HBED), and 1 mmol Fe<sup>3+</sup>, the pH being fixed at a given value for each run. The pH values were set by addition of trace amounts of strong acid or base to a volume of 15 mL of solution and the solutions were allowed to equilibrate for 24 h. In each experiment, the UV/vis spectra of the iron complexes as a function of pH were obtained from a single solution. A spectrum was recorded after each pH adjustment. The values of the stability constants are the average values of three experiments. The overall metal-complex stability constant was determined by competition studies with the hexadentate ligand HBED by spectrophotometric methods and calculated using the program pH AB 2006 [23]. Distribution diagrams were plotted using the program Hyss 2006 [24].

#### Fluorescence measurements

Fluorescence measurements were performed with a Varian Cary Eclipse spectrofluorometer equipped with a Varian Peltier single cell holder, in 1-cm cuvettes. All the spectra were recorded at 37 ± 0.1 °C, with excitation and emission slit widths of 0.05 m and with an exposure time of 4,000 s, in the range from 500 to 700 nm for emission and at 496 nm for excitation for **5** and from 565 to 750 nm for emission and at 561 nm for excitation for **4**.

Stock solutions of the different compounds were obtained by preparing a saturated solution of the compound in dimethyl sulfoxide (DMSO). Samples for fluorescence measurements were prepared by dilution of a known volume of the DMSO stock solution in 10 mM 3-(*N*-morpholino)propanesulfonic acid (MOPS) buffer solution. The percentage of the DMSO stock solution was always less than 1% in the final volume.

#### Fluorescence quenching

Fluorescence quenching measurements were performed in MOPS buffer at 37 °C. Stock solutions of the different

metal ions were acquired [Fe(NO<sub>3</sub>)<sub>3</sub>, Ca(NO<sub>3</sub>)<sub>2</sub>, Cu(NO<sub>3</sub>)<sub>2</sub>, Mg(NO<sub>3</sub>)<sub>2</sub>, Zn(NO<sub>3</sub>)<sub>2</sub>, Mn(NO<sub>3</sub>)<sub>2</sub> and Ni(NO<sub>3</sub>)<sub>2</sub>] from Sigma–Aldrich. A saturated solution of **4** in DMSO was prepared and used as a stock solution. To prepare the solution for fluorescence measurements, a known volume of the stock solution was diluted with MOPS buffer to achieve a final concentration of **4** of 3 × 10<sup>-6</sup> M. The percentage of the DMSO stock solution was always less than 1% in the final volume. The probe solution was then mixed with increasing amounts of the metal stock solution, in a range of molar ratios from 1:0.2 to 1:2 of **4** to metal ion. All measurements were performed using a Varian Cary Eclipse spectrofluorimeter.

The values of the fluorescence quantum yield of the fluorescent chelators **4** and **5** and rhodamine B were determined according to the method of Williams et al. [25] using fluorescein as the standard. To minimize reabsorption effects, the values of the absorbance in the fluorescence cuvette were maintained below 0.1 at and above the excitation wavelength.

#### Liposome preparation

Liposomes were prepared by evaporation to dryness with a stream of argon of a lipid solution in chloroform (dimyristoylphosphatidylcholine; DMPC) or in chloroform/methanol (1:1) (dimyristoylphosphatidylglycerol; DMPG). The lipids DMPC and DMPG were purchased from Avanti Polar Lipids (Alabaster, AL, USA). The films were maintained under a vacuum, for a minimum of 3 h to remove all traces of the organic solvent. The resulting dried lipid films were dispersed with 10 mM MOPS buffer (0.1 M NaCl, pH 7.4), and the mixture was vortexed above the phase-transition temperature (37 ± 0.1 °C) to produce multilamellar liposomes. The multilamellar liposomes were then subjected to the following cycle five times: freeze vesicles in liquid nitrogen and thaw in a water bath at 37 ± 0.1 °C. Lipid suspensions were equilibrated at 37 ± 0.1 °C for 30 min and extruded ten times through polycarbonate filters (100 nm) to produce large unilamellar vesicles. Extrusion of liposomes was performed with a Lipex Biomembranes (Vancouver, Canada) extruder attached to a circulating water bath. The size distribution of extruded DMPC liposomes, with and without added compound, was determined by dynamic light scattering analysis using a Malvern Instruments Zetasizer nano ZS. Lipid concentrations in vesicle suspensions were determined by phosphate analysis, using a modified version of the Fiske and Subbarow [26] method. Chelator solutions were added to liposome suspensions and vortexed for 5 min followed by incubation at 37 °C for 30 min. Two sets of nine samples (1.5 mL) were typically used in each experiment.

### Partition constants

$K_p$  values for the liposome distribution of fluorophores were determined using the equation  $\Delta I = (\Delta I_{\max}[\text{lipid}] / (1/K_p\gamma) + [\text{lipid}])$ , in which  $I$  is the fluorescence intensity of the fluorophore in the presence of lipid vesicles and  $I_0$  is the fluorescence intensity in its absence,  $\Delta I = I - I_0$ ,  $\Delta I_{\max} = I_{\infty} - I_0$  is the maximum difference in fluorescence intensity,  $I_{\infty}$  represents the limiting value of  $I$ , and  $\gamma$  is the molar volume of the lipid [27].

Values of  $\log P$  were calculated using the Molinspiration software suite (version 2.2) (<http://www.molinspiration.com>).

### Cell culture and reagents

Bone-marrow-derived macrophages (BMM $\phi$ ) were isolated from the femurs and tibias of 6–8-week-old C57BL/6 mice (Harlan Bioproducts, Bicester, UK) using standardized procedures. Cells were plated in Dulbecco's modified Eagle's medium (Invitrogen, Paisley, UK) supplemented with 10% heat-inactivated fetal calf serum (Sigma–Aldrich, UK), 5% horse serum (Invitrogen), 1% L-glutamine (Invitrogen) and 20% L929 cell culture supernatant as a source of macrophage colony-stimulating factor. Cells were cultivated at 37 °C and 7.5% CO<sub>2</sub>. Mature adherent macrophages were harvested after 7 days of culture and stored at –80 °C in 10% DMSO to be replated when required. Thawed cells were cultured overnight and non-adherent cells were washed off prior to manipulations. No antibiotics were used in the cell culture medium. Phosphate-buffered saline (PBS) (pH 7.4, Invitrogen) and block buffer (1% bovine serum albumin, 5% heat-inactivated horse serum, 0.05% sodium azide in PBS, pH7.4) were treated with Chelex-100 (sodium form, Sigma–Aldrich, Gillingham, UK) to remove iron contamination.

### Flow cytometry

For flow cytometry measurements, non-adherent cells were washed off from cultivated cell monolayers, which were subsequently incubated for 20 min in cold PBS. The cells were scraped off the plates, washed with PBS and split into flow cytometry tubes at 10<sup>5</sup> cells per tube. For cellular iron loading and deprivation, cells were incubated for 50 min at 37 °C and 7.5% CO<sub>2</sub> in 500  $\mu\text{g}/\text{mL}$  iron(III) ammonium citrate (Sigma–Aldrich) and in 100  $\mu\text{mol}$  deferoxamine mesylate (DFO; Sigma–Aldrich), deferasirox (DFR; Exjade<sup>®</sup>) or deferiprone (DFP; Ferriprox<sup>®</sup>), respectively. Following washing with cold PBS, the cells were incubated with **4**, provided as a 10 mM stock solution in DMSO and diluted in PBS to a final concentration of 10  $\mu\text{M}$ , for 20 min at 37 °C and 7.5% CO<sub>2</sub>. The cells were washed and

resuspended in cold PBS. Measurements were carried out using an FACSCalibur flow cytometer (BD Biosciences, Oxford, UK). Analysis proceeded via Cell-Quest and FlowJo software programs. Gates were based on dot plots of untreated cell populations. The median fluorescence of at least 10,000 events was recorded and corrected for cell autofluorescence. Mean values were calculated for medians of three independent experiments.

### Confocal microscopy

For live cell imaging of intracellular probe distribution, BMM $\phi$  were plated onto sterile cover slips in six-well plates at 10<sup>5</sup> cells per cover slip and left to settle overnight. For lysosomal labelling, fluorescein-conjugated or Texas Red conjugated dextran (Invitrogen) was added at 100  $\mu\text{g}/\text{mL}$  for 4 h, and subsequently chased overnight with cell medium. For phagosomal labelling, cells were incubated with fluorescein-conjugated zymosan (Invitrogen) or with Dynabeads<sup>®</sup> M-280 Tosylactivated (Invitrogen) for 20 min. Cells were washed with PBS and incubated for 20 min with 10  $\mu\text{mol}$  **4** or 100  $\mu\text{mol}$  **5** in PBS, simultaneously with fluorescein-conjugated or Texas Red conjugated dextran for endosomal labelling, or with MitoTracker<sup>®</sup> Green FM or MitoTracker<sup>®</sup> Deep Red 633 (Invitrogen) for mitochondria, or with Cy3-conjugated transferrin (transferrin-Cy3) (Invitrogen) for early and recycling endosomes. The cells were washed with cold PBS. For surface labelling, cells were incubated in cold block buffer for 20 min, followed by 20-min incubation with Cy5-conjugated anti-mouse CD11b (Abcam, Cambridge, UK, 1:200, in block buffer) with a subsequent wash with PBS.

Fluorescence was visualized using an inverted Zeiss confocal fluorescence microscope and a  $\times 63$  oil immersion objective. Images were acquired by Zeiss LSM Image Browser.

## Results

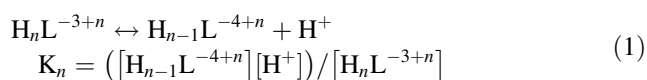
### Design of iron chelators

The hexadentate chelators reported in the present work were designed to be evaluated as iron deprivation agents to target infection processes induced by *Mycobacteria*. Also, when designing the potential antimicrobial agents, we considered the possibility of introducing into the chelator framework fluorescent labels that could allow its pathways in the cell to be followed by fluorescence microscopy a priority. To synthesize the hexadentate chelators we linked three bidentate 3-hydroxy-4-pyridinone moieties (**1**) to a selected tripodal anchor based on a tetrahedral carbon

atom (2) (Scheme 1). The use of this particular tripodal molecule permits the addition of other functional groups such as fluorophores. Compound **2** had previously been conjugated via amide bonds to produce iron-binding dendrimers [21] and polymers [28], and in the present work an analogous procedure was adopted to prepare iron chelators **3**, **4** and **5** (Scheme 1). The hexadentate chelating unit, common to **3**, **4** and **5**, is built from 3-hydroxy-4-pyridinone molecules which provide for iron(III) an octahedral coordination sphere, as shown in Fig. 1 for **4**. The choice of ligand (**1**) that binds to the anchor (**2**) via the *ortho* position was made to ensure that the resulting hexadentate molecule unit possesses a high affinity for iron(III) [29, 30]. Compound **3** is essentially the hexadentate chelating unit which has been blocked from further substitution to facilitate the physicochemical characterization of the hexadentate unit. Compound **4** is a fluorescent hexadentate chelator prepared by coupling the chelating unit with rhodamine B, a fluorophore which has a lipophilic character and contrasts with green-labelled bacteria used in the infection model studies. Compound **5** is an analogous fluorescent hexadentate chelator, which contains the fluorescein core.

#### Speciation and affinity for iron

Information relating to the predominant ligand species at physiological pH values and the affinity constant for iron are essential for a clear comprehension of the distribution of iron chelating molecules. Owing to interference arising from the fluorophores in both potentiometric and spectrophotometric measurements, we isolated the hexadentate chelating unit **3**, common to all the chelators, to determine the dissociation constants of the ligand and its affinity constant for iron(III). Compound **3** was obtained as a hydrochloride which in strong acidic solution can be represented as  $H_6L^{3+}$  and which has six dissociable protons that are displaced according to Eq. 1 for  $6 \leq n \leq 1$ .



The acid–base properties of **3** were investigated by both potentiometric and spectrophotometric methods. Fitting analysis of the titration curves was achieved using the program Hyperquad [25] and led to the determination of six  $pK_a$  values:  $pK_{a1} = 2.44 \pm 0.01$ ;  $pK_{a2} = 3.08 \pm 0.04$ ;  $pK_{a4} = 3.78 \pm 0.07$ ;  $pK_{a4} = 8.57 \pm 0.09$ ;  $pK_{a5} = 9.21 \pm 0.11$ ;  $pK_{a6} = 9.80 \pm 0.18$ . These were found to be consistent for the two methods. The values obtained can be grouped into two sets, centred at the values 3 and 9, which are the typical  $pK_a$  values found for bidentate 3-hydroxy-4-pyridinones [31]. The values are in close agreement with those of other 3-hydroxy-4-pyridinone

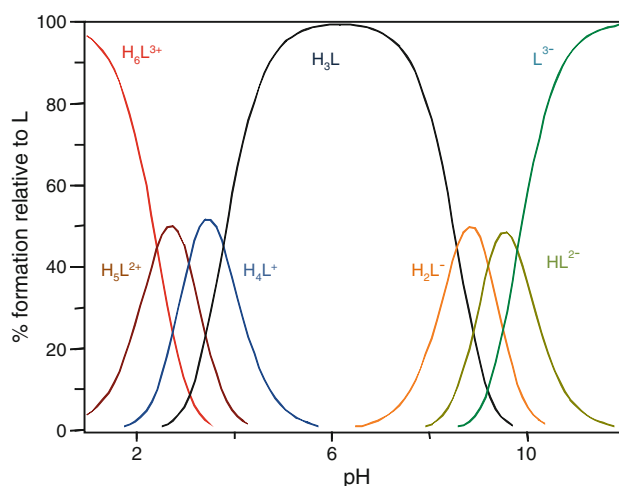


**Fig. 2** Speciation plot for hexadentate chelator **3**, as a function of pH

hexadentate chelators which have been prepared using different molecular frameworks [32]. The neutral species  $H_3L$  dominates over the pH range 4–9 and its molar fraction is 96% at pH 7.4 (Fig. 2) [24].

The high affinity of this ligand for iron(III) is confirmed by the UV/vis spectra of solutions of the ligand in the presence of iron(III) which show a characteristic ligand to metal charge transfer band of the iron(III) complex even at low pH values (Fig. S1). The overall affinity constant of **3** for iron was determined by competition studies against the ligand HBED using UV/vis spectroscopy as previously described [33–36]. The  $\log \beta(Fe^{3+})$  and  $pFe^{3+}$  values (calculated as  $-\log[Fe^{3+}]$  at pH 7.4 with a total ligand concentration of  $10^{-5}$  M and a total Fe(III) concentration of  $10^{-6}$  M [37]) obtained for **3** were  $34.4 \pm 0.1$  and 29.8, respectively. Different values for  $\log \beta(Fe^{3+})$  and  $pFe^{3+}$  have been previously reported [21], and were based on erroneously estimated  $pK_a$  values. The values of  $\log \beta$  and  $pFe^{3+}$  of **3** are compared with those of a range of siderophores in Table 1. It is clear that chelator **3** and related compounds are good candidates to deprive bacteria of iron. Indeed the very strong capacity to chelate iron is a major determinant for the antibacterial activity of **4** since it has been demonstrated that the iron(III) complex is an ineffective antimycobacterial agent [11].

#### Fluorescence properties

The fluorescence properties of **4** and **5** were studied in aqueous solution over the pH range 5–9 (Table 2). The values of the fluorescence quantum yields ( $\Phi$ ) determined for chelators **4** and **5** are lower than those of the correspondent fluorophores. For **4** we investigated the influence of  $Fe^{3+}$ ,  $Zn^{2+}$ ,  $Cu^{2+}$ ,  $Ni^{2+}$ ,  $Mn^{2+}$ ,  $Ca^{2+}$  and  $Mg^{2+}$  on its fluorescence intensity. The results obtained in  $3 \mu M$

**Table 1** Affinity constants and  $pFe^{3+}$  values for chelator **3**, deferoxamine and siderophores produced by mycobacteria

Siderophore	Ligand architecture	$\log \beta$	$pFe^{3+}$	Reference
<b>3</b>	Tripodal, 3-hydroxy-4-pyridinone	34.40	29.84	This work
Mycobactin	Linear, bishydroxamate, <i>N</i> -(oxazoline) and OH(salicylic acid)	31	29.0	– <sup>a</sup>
Cell-wall-associated mycobacteria siderophores				
Carboxymycobactin	Linear, bishydroxamate, <i>N</i> -(oxazoline) and OH(salicylic acid)	31	29.0	– <sup>a</sup>
Extracellular mycobacteria siderophores				
Exochelin MN	Linear, bishydroxamate, three- $\beta$ -hydroxylhistidine	39.10	31.10	[44]
<i>Mycobacterium neoaurum</i> siderophore				
Exochelin MS	Linear, trishydroxamate	28.90	25.00	[35]
<i>Mycobacterium smegmatis</i> siderophore				
Deferoxamine	Linear, trishydroxamate	31.00	26.60	[45]
<i>Actinobacter Streptomyces pilosus</i> siderophore				

<sup>a</sup> Calculated with the software suite Marvin & Marvin version 5.1.4 [43]

solutions of chelator **4** together with a 1:1 molar ratio of metal ion are shown in Fig. 3. The values are the mean values obtained in three independent experiments and the associated standard deviation is 0.1%. From analysis of the figure it is clear that  $Ca^{2+}$  and  $Mg^{2+}$  do not influence the fluorescence intensity, whereas  $Fe^{3+}$ ,  $Zn^{2+}$ ,  $Cu^{2+}$ ,  $Ni^{2+}$  and  $Mn^{2+}$  induce fluorescence quenching. Although fluorescence quenching of **4** in the presence of  $Cu^{2+}$  and  $Zn^{2+}$  is appreciable at equivalent concentrations, under physiological conditions the cytoplasmic levels of low molecular weight complexes of  $Cu^{2+}$  and  $Zn^{2+}$  are much lower than those of  $Fe^{3+}$ , these values typically being less than  $10^{-15}$  M  $Cu^{2+}$  [38], less than  $10^{-9}$  M  $Zn^{2+}$  [39] and approximately  $10^{-6}$  M  $Fe^{3+}$  [40]. Thus, in living cells, we believe that any observed contribution of metal ion chelation to the fluorescence quenching of **4** is likely to be associated with the presence of chelatable iron. Evidence that formation of the corresponding metal complexes is a significant contribution to fluorescence quenching is provided by experiments performed with different concentrations of the metal ion. For iron(III), the maximal fluorescence quenching is achieved at a 1:1 molar ratio (Fig. S2). A profile of fluorescence quenching in the presence of different concentrations of the biologically relevant metal ions  $Fe^{3+}$ ,  $Zn^{2+}$  and  $Cu^{2+}$  is depicted in Fig. S3. The quenching profiles evidence the different behaviour of the paramagnetic metal ions  $Fe^{3+}$  and  $Cu^{2+}$  and diamagnetic  $Zn^{2+}$  concerning the contribution to fluorescence quenching.

#### Partition studies

Conventional partition coefficients were not directly determined because of the difficulty of the measurement of the  $pK_a$  values of both **4** and **5**, thus preventing reliable conversion of  $\log D_{7.4}$  values to  $\log P$  values. The  $clog P$  values revealed that the rhodamine-labelled chelator (**4**) is

**Table 2** Spectroscopic data of fluorescent compounds

	UV/vis		Fluorescence	
	$\lambda_{max}$ (nm)	$\epsilon$ ( $M^{-1} cm^{-1}$ )	$\lambda_{max}$ (nm)	$\Phi$
<b>4</b>	561	$2.80 \times 10^4$	582	0.027
<b>5</b>	496	$6.34 \times 10^4$	520	0.171
Rhodamine B	543	$1.06 \times 10^5$	550	0.310
Fluorescein	498	$9.23 \times 10^4$	425	0.950

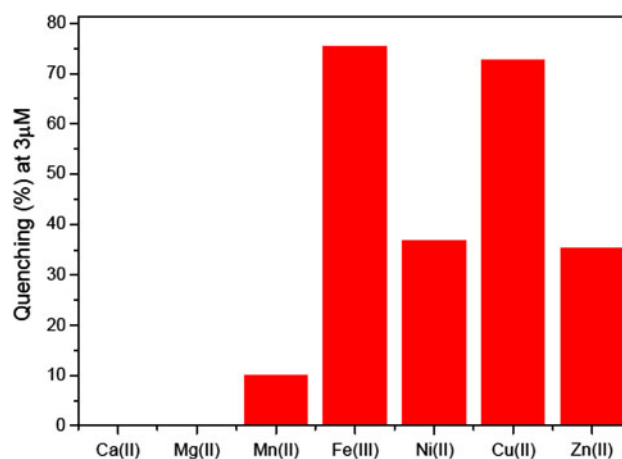


**Fig. 3** Influence of  $Fe^{3+}$ ,  $Zn^{2+}$ ,  $Cu^{2+}$ ,  $Ni^{2+}$ ,  $Mn^{2+}$ ,  $Ca^{2+}$  and  $Mg^{2+}$  on the fluorescence intensity of chelator **4**. The results were obtained in 10 mM 3-(*N*-morpholino)propanesulfonic acid solution (pH 7.4) of 3  $\mu$ M chelator **4** together with a 1:1 molar ratio of different metal ions

more hydrophobic than the fluorescein-labelled chelator (**5**), the  $clog P$  values being 1.731 and 0.042, respectively.

In an attempt to investigate this difference in greater detail, partition experiments were undertaken in liposome suspensions, using DMPC and DMPG. For both the rhodamine-labelled chelator (**4**) and rhodamine B, the fluorescence intensity was observed to be significantly

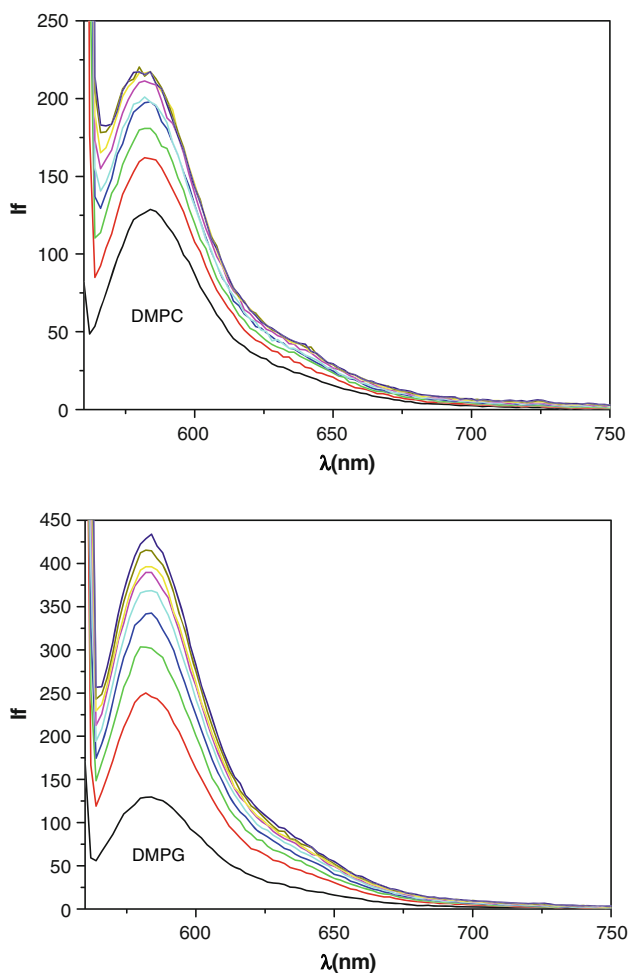


**Fig. 4** Fluorescence intensity observed for 2.85  $\mu\text{M}$  solutions of chelator **4** in the presence of suspensions of dimyristoylphosphatidylcholine (DMPC) and dimyristoylphosphatidylglycerol (DMPG) large unilamellar vesicles prepared with lipid concentrations indicated by the following colour code: black 0.0  $\mu\text{M}$ , red 134  $\mu\text{M}$ , green 267  $\mu\text{M}$ , blue 401  $\mu\text{M}$ , cyan 536  $\mu\text{M}$ , magenta 670  $\mu\text{M}$ , yellow 803  $\mu\text{M}$ , dark yellow 933  $\mu\text{M}$ , navy 1,080  $\mu\text{M}$

enhanced in the presence of large unilamellar vesicles (Fig. 4). The fluorescence intensity of rhodamine B is known to be perturbed by the presence of other molecules able to interact with the xanthene chromophore. In a study of the fluorescence properties of rhodamine B in the presence of cyclodextrins, it was shown that the fluorescence intensity can be either quenched or enhanced depending on which of two distinct binding sites is preferred by cyclodextrins [41]. The observation of a significant enhancement of the fluorescence intensity of chelator **4** is thus assigned to its interaction with the lipid phase provided by liposomes. No such enhancement was observed with either the fluorescein-labelled chelator (**5**) or fluorescein itself, presumably because they did not interact with the liposome preparations. This finding is in agreement with the two estimated log  $P$  values. The fluorescence data obtained for liposome

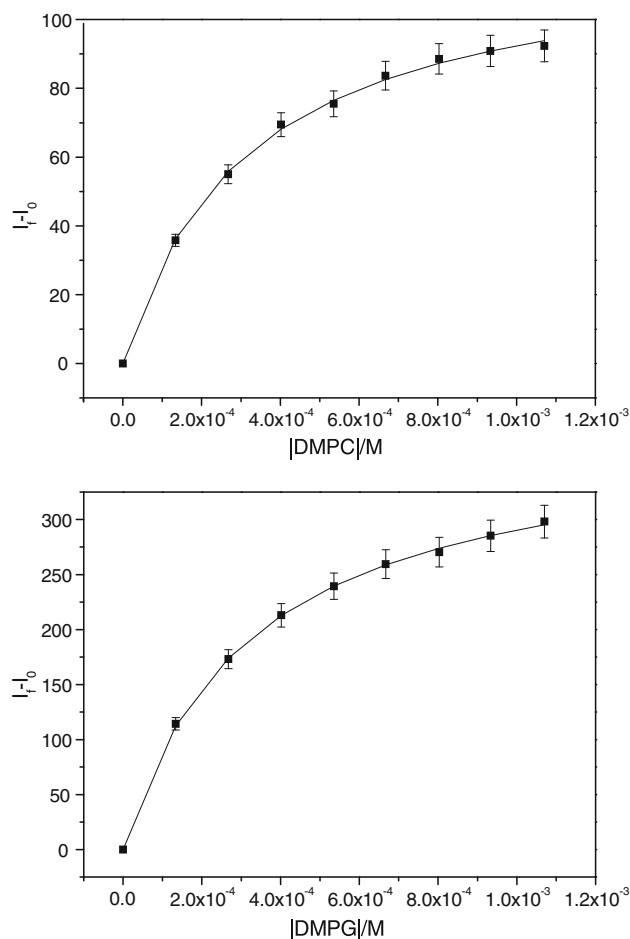


**Fig. 5** Fitting of fluorescence intensity parameters of chelator **4** according to the equation  $\Delta I = (\Delta I_{\max}[\text{lipid}]/(1/K_P\gamma) + [\text{lipid}])$ , in which  $I$  is the fluorescence intensity of the fluorophore in the presence of lipid vesicles and  $I_0$  is the fluorescence intensity in its absence,  $\Delta I = I - I_0$ ,  $\Delta I_{\max} = I_{\infty} - I_0$  is the maximum difference in fluorescence intensity,  $I_{\infty}$  represents the limiting value of  $I$ , and  $\gamma$  is the molar volume of the lipid [27]. Log  $K_P$  values for **4**: DMPC, 3.71; DMPG, 3.79

preparations of **4** are presented in Fig. 5. The log  $K_P$  values in DMPC and DMPG were determined as 3.71 and 3.79. These values are similar to the corresponding values obtained for rhodamine B, namely 3.76 and 3.84, which confirms that **4** and rhodamine B interact strongly with both zwitterionic and negatively charged lipid membranes. Rhodamine B has a marginally greater degree of partition in the membrane phase when compared with the partition of **4**, indicating that it is this portion of the molecule which enjoys the favourable interaction with the lipid surface.

#### Macrophage studies

##### *Intracellular distribution of fluorescent labelled chelators*

The intracellular distribution of the fluorescent chelators was analysed in BMMØ from C57BL/6 mice. These

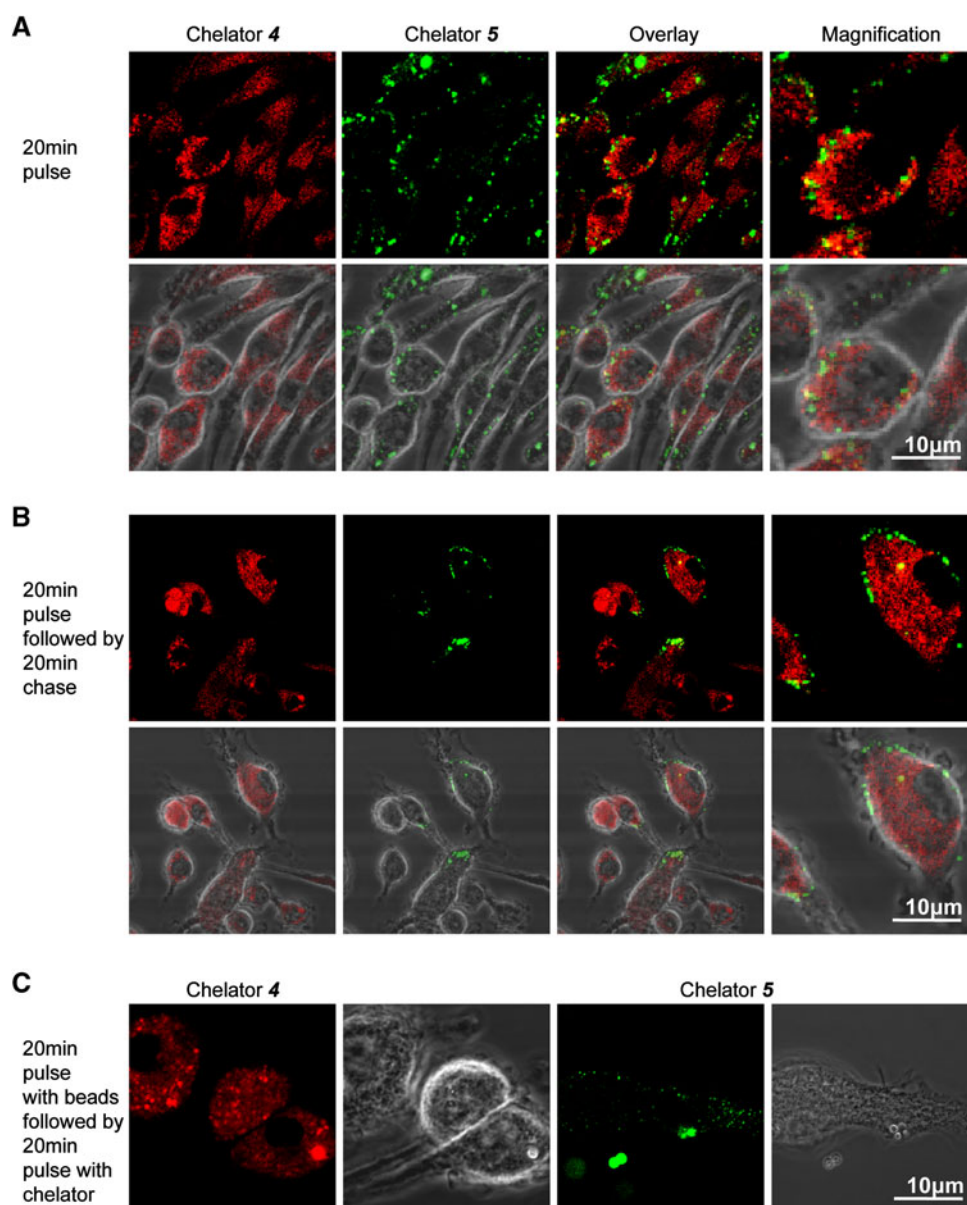


**Fig. 6** Representative confocal microscopy images of intracellular distribution and colocalization studies of chelators **4** and **5** in bone-marrow-derived macrophages (BMMØ). Cells were incubated with individual solutions of **4** or **5** or with combined chelators in iron-free phosphate-buffered saline (PBS). From titration experiments where cells were incubated with increasing chelator concentrations, comparable fluorescence intensity was observed for **4** (10  $\mu\text{M}$ ) and **5** (100  $\mu\text{M}$ ). Cells were incubated simultaneously with **4** (10  $\mu\text{M}$ ) and **5** (100  $\mu\text{M}$ ) for 20 min, and the intracellular chelator distribution was monitored immediately (**a**) and upon a 20-min chase with PBS (**b**). To

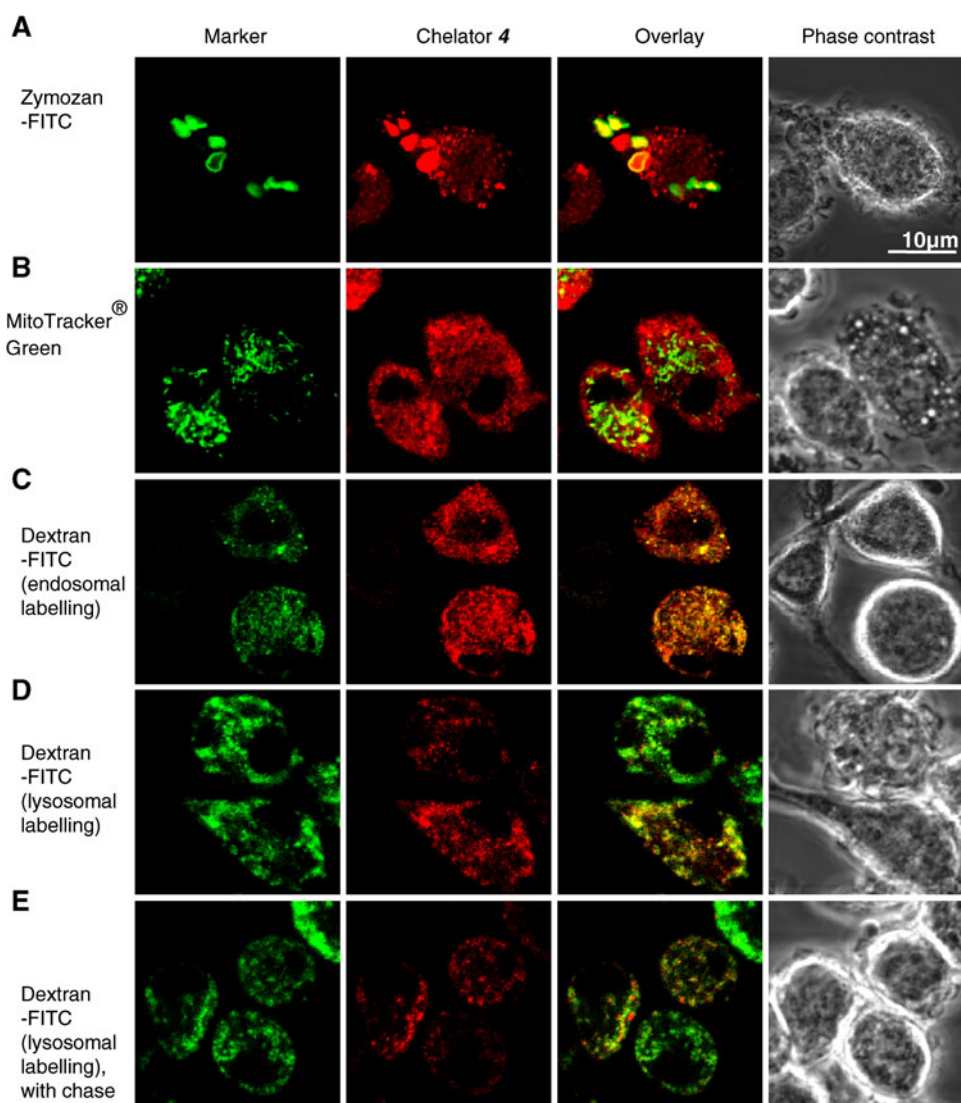
characterize the access of chelators **4** and **5** to phagosomes, colocalization studies were performed using Dynabeads as phagosome markers. Cells were incubated with Dynabeads<sup>®</sup> M-280 Tosylactivated (Invitrogen) for 20 min, washed with PBS and incubated for 20 min with 10  $\mu\text{M}$  **4** or 100  $\mu\text{M}$  **5** in PBS (**c**). Fluorescence of stained cells was measured in the green as well as in the red channel, and data were merged for evaluation of colocalization in *yellow*. Fluorescence data are shown in comparison with the corresponding bright-field images. Magnification of merged fluorescence data show detailed colocalization

adherent cells were incubated with individual solutions of **4** or **5** or with combined chelators in iron-free PBS. From titration experiments where cells were incubated with increasing chelator concentrations, comparable fluorescence intensity was observed for **4** (10  $\mu\text{M}$ ) and **5** (100  $\mu\text{M}$ ). Considering the quantum yields determined for

the two compounds in buffer solution at pH 7.4 (Table 2), this result was not to be expected.

Cells were pulsed simultaneously with **4** (10  $\mu\text{M}$ ) and **5** (100  $\mu\text{M}$ ), and the intracellular chelator distribution was monitored immediately (Fig. 6a) and upon a 20-min chase with PBS (Fig. 6b). After 20 min of incubation, **4** was

**Fig. 7** Representative confocal microscopy images of intracellular colocalization studies of chelator **4** and phagosomal (a), mitochondria (b), endosomal (c) and lysosomal markers (d, e) in BMMØ. For phagosomal, mitochondrial, and endosomal labelling, cells were incubated for 20 min with fluorescein-labelled zymosan (*zymosan-FITC*), MitoTracker Green FM and fluorescein-labelled dextran (*dextran-FITC*), respectively. For lysosomal labelling, dextran-FITC (Invitrogen) was added at 100 µg/mL for 4 h, and subsequently chased overnight with cell medium. Cells were washed with PBS and incubated with chelator **4** (10 µM) for 20 min. Fluorescence of stained cells was measured in the green as well as in the red channel, and data were merged for evaluation of colocalization in *yellow*. Fluorescence data are shown in comparison with the corresponding bright-field images



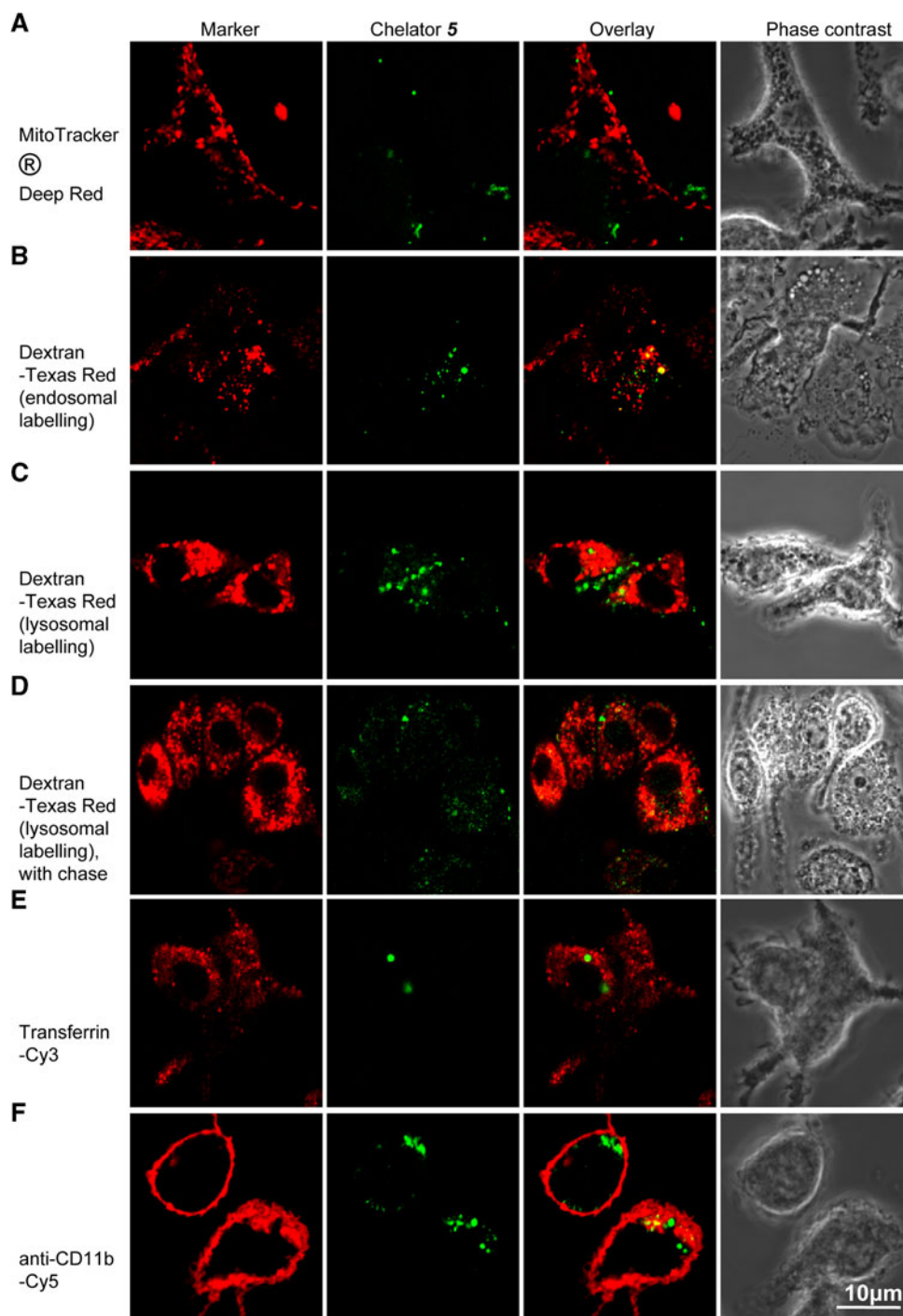
readily visualized within the macrophages, whereas **5** was found at the periphery of the cells, revealing the distinctly different intracellular distribution of both chelators early after uptake. Only after a chase of an additional 20 min did both chelators partially colocalize within the cells, indicating differential pathways and/or kinetics of internalization for both chelators.

To characterize the intracellular compartments targeted by the chelators, colocalization studies were performed using (1) fluorescein-labelled zymosan and Dynabeads as phagosome markers, (2) fluorescein-conjugated and Texas Red conjugated dextran for endosomes and lysosomes and (3) MitoTracker Green FM and MitoTracker Deep Red 633 as mitochondrial markers. Both **4** and **5** have access to bead-containing phagosomes, following 20-min incubation with the chelators (Fig. 6c), indicating at least partial intersection with the endosome/phagosome system. Similar

to bead-containing phagosomes, **4** also accessed fluorescein-conjugated zymosan phagosomes (Fig. 7a). Colocalization of **4** with the zymosan surface suggested chelator accumulation in the yeast cell wall fragments (zymosan), which was confirmed by incubation of free zymosan with **4** strongly labelling the zymosan particles.

Colocalization patterns acquired after 20-min incubation of macrophages with chelators and simultaneously with MitoTracker Green FM or MitoTracker Deep Red 633 revealed that neither chelator accesses mitochondria (Figs. 7b, 8a). Simultaneous incubation of macrophages with **4** and the endosomal tracer fluorescein-labelled dextran showed that **4** accessed endosomes and subsequently lysosomes (Fig. 6c vs. d, e). In contrast, only a small proportion of **5** colocalized with Texas Red conjugated dextran labelled endosomes and lysosomes (Fig. 8b–d). Compound **5** accumulated predominantly in vesicles at the

**Fig. 8** Representative confocal microscopy images of intracellular colocalization studies of chelator **5** and mitochondria (a), endosomes (b) and lysosomes (c, d) in BMMØ. The procedure is as described in the legend to Fig. 6 but used a concentration of chelator **5** of 100  $\mu$ M and MitoTracker Deep Red 633 and Texas Red conjugated dextran. For the imaging of early and recycling endosomes, cells were incubated with Cy3-conjugated transferrin (e). For surface labelling, cells were incubated in cold block buffer for 20 min, followed by 20-min incubation with Cy5-conjugated anti-mouse CD11b (f). Fluorescence of stained cells was measured in the green as well as in the red channel, and data were merged for evaluation of colocalization in yellow. Fluorescence data are shown in comparison with the corresponding bright-field images



cell surface, whereas **4** spread throughout the endosomal/lysosomal system of the cells.

The cellular distribution, kinetics of uptake and colocalization patterns of the fluorescein-labelled hexadentate chelator **5** are similar to those previously observed for a fluorescein-labelled bidentate pyridinone probe [42]. Both compounds appear to remain localized at the cell surface after 20-min incubation; however, the bidentate pyridinone

probe is further chased into lysosomes, whereas the majority of **5** remains in vesicles or membrane moieties at the cell surface.

The intracellular localization of **5** was further studied using the early/recycling endosome tracer transferrin-Cy3 and the surface marker CD11b (Fig. 8e, f). After a 20-min incubation, **5** did not colocalize with early endosomes (Fig. 8e) but colocalize partially with the marker CD11b

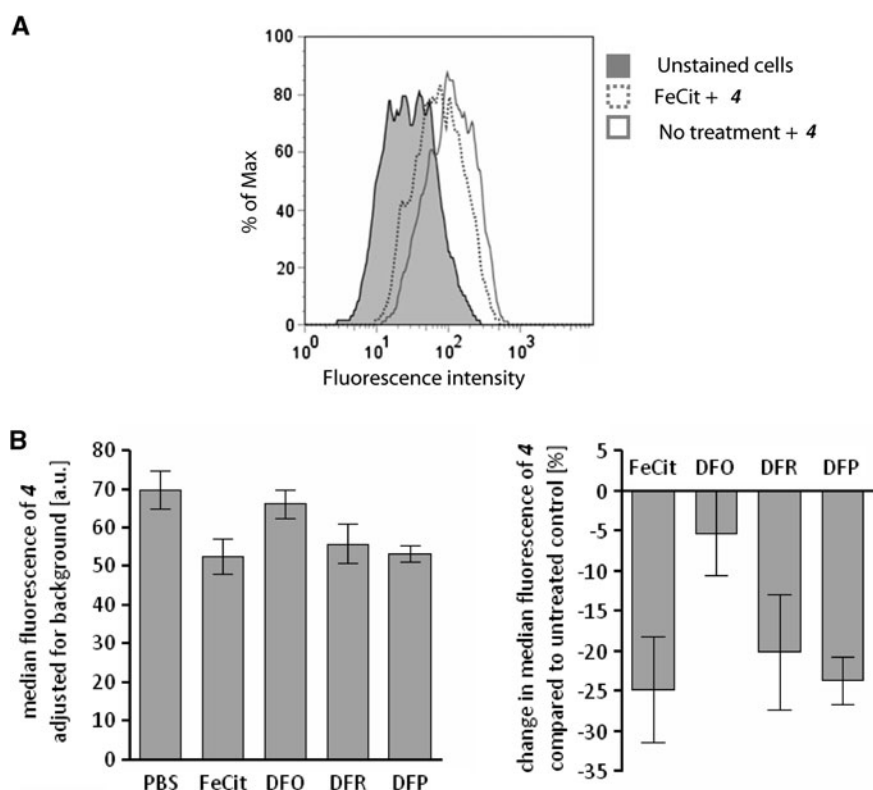


**Fig. 9 a** Representative flow cytometry histograms of chelator **4** in BMMØ. Cells were incubated with **4**, at a final concentration of 10 µmol, for 20 min at 37 °C and 7.5% CO<sub>2</sub>. The cells were washed and resuspended in cold PBS. For cellular iron loading, cells were incubated for 50 min at 37 °C and 7.5% CO<sub>2</sub> in 500 µg/mL iron(III) ammonium citrate following washing with cold PBS. Cells were incubated with **4**, at a final concentration of 10 µmol, for 20 min at 37 °C and 7.5% CO<sub>2</sub>. The cells were washed and resuspended in cold PBS. We used the designations “unstained cells” for macrophages, “no treatment” for macrophages incubated with **4** and “FeCit” for macrophages treated with iron(III) citrate and incubated with **4**. Data

were acquired in the red channel. Gates were based on dot plots of untreated cell populations. **b** Responsiveness of intracellular chelator **4** in iron-overloaded and iron-deprived BMMØ. For cellular iron loading and deprivation, cells were incubated for 50 min at 37 °C and 7.5% CO<sub>2</sub> in 500 µg/mL iron(III) ammonium citrate and in 100 µmol deferoxamine mesylate (DFO), deferasirox (DFR) and deferi-prone (DFP), respectively, following washing with cold PBS. Cells were incubated with **4**, at a final concentration of 10 µmol, for 20 min at 37 °C and 7.5% CO<sub>2</sub>. The cells were washed and resuspended in cold PBS. Data were acquired in the red channel. Gates were based on dot plots of untreated cell populations

(Fig. 8f), suggesting association with membrane moieties distinct from endocytic entry sites.

#### Intracellular iron sensitivity of **4** under iron overload and deprivation

The intracellular fluorescence of **4** was analysed in vitro by flow cytometry using BMMØ from C57BL/6 mice. All flow cytometry analyses were carried out in Chelex-treated PBS to avoid external iron contamination. As shown in Fig. 9a, **4** is efficiently endocytosed by macrophages, leading to an increase in intracellular fluorescence when compared with unlabelled cells. Chelator sensitivity was investigated under conditions of iron overload by adding iron citrate or iron deprivation by DFO, DFR and DFP. Iron overload induced a significant decrease of fluorescence intensity when compared with untreated cells (Fig. 9a, b).

This observation confirms that the chelator has access to citrate-delivered iron and cellular compartments susceptible to fluctuations in iron levels.

Iron deprivation by the chelators DFR and DFP caused a significant decrease in fluorescence intensity of **4**, whereas treatment with DFO resulted in a less significant fluorescence decrease. To explain the differential responsiveness of **4**, both thermodynamic and kinetic arguments have to be considered. According to the pFe<sup>3+</sup> values (29.8 for **4**, 26.6 for DFO, 22.5 for DFR, 19.5 for DFP), chelator **4** has the highest affinity for iron, followed by DFO, DFR and DFP. Thermodynamically, chelator **4** is expected to displace iron(III) from the three complexes. However, from the kinetic point of view it is known that complexes formed by tridentate and bidentate ligands are much more labile than those formed by hexadentate chelators. This tendency may explain the fact that in the same period of time of

incubation with chelator **4** the decrease in fluorescence is much more evident for DFR and DFP. The flow cytometry results indicate that, within the intracellular environment, chelator **4** is able to displace iron(III) from other complex forms.

## Discussion

The speciation plot of **3** demonstrates that the hexadentate moiety is neutral over the pH range 4–9 (Fig. 2), thus indicating that the net charge of chelator probes **4** and **5** is dominated by the respective chromophores, chromophore **4** being zwitterionic and **5** being negatively charged. Probes **4** and **5** contain the hexadentate chelating unit of **3** and thus have similar affinity for iron(III). The latter is of the same magnitude as that exhibited by mycobacterium siderophores (Table 1). Both **4** and **5** are selective for iron(III) under biological conditions.

As demonstrated by the values of *clog P* and the liposome partition studies, probe **4** is strongly lipophilic in contrast to **5**. Thus, from consideration of the physicochemical characterization of **4** and **5**, neither of the compounds would be predicted to readily cross membranes by non-facilitated diffusion but **4** is predicted to be strongly surface active.

In macrophages, the intracellular distribution of **4** and **5** was markedly different. Probe **4** became widely distributed in the cell within 20 min, accumulating in phagosomes, endosomes, and finally predominantly in lysosomes but not in mitochondria. Probe **5** localized to vesicles and membrane moieties proximal to the plasma membrane but not to phagosomes, endosomes, lysosomes nor mitochondria. It is likely that probe **4** remains largely membrane bound when distributing throughout the cell endocytic pathway. However, the chelating portion of the molecule is predicted to be exposed to the lumen of the organelles to allow iron scavenging from the aqueous phase. This property was confirmed by a cell sorting study, where it was demonstrated that within macrophages probe **4** was able to remove iron from both DFP and DFR. Competition with DFO was much less effective. However, this was to be expected as competition between hexadentate chelators is remarkably slow even at pH 5.5.

Thus, it is likely that probe **4** will be able to successfully compete with carboxymycobactins and mycobactins for iron, thereby offering a mechanism for the observed antimycobacterial effect. Once iron is bound to probe **4**, natural siderophores would be predicted to experience considerable difficulty in scavenging this iron. Competitive interference with mycobacterial siderophores by exogenous iron chelators offers an effective antimicrobial strategy with potential to combat infections, including tuberculosis.

**Acknowledgments** Financial support from FCT-Fundação para a Ciência e Tecnologia, Portugal, through projects POCI/QUI/56214/2004 and PTDC/QUI/67915/2006 is gratefully acknowledged.

## References

- Marx JJ (2002) *Best Pract Res Clin Haematol* 15:411–426
- Ratledge C (2004) *Tuberculosis* 84:110–130
- Ratledge C, Dover LG (2000) *Annu Rev Microbiol* 54:881–941
- De Voss JJ, Rutter K, Schroeder BG, Barry CE (1999) *J Bacteriol* 181:4443–4451
- Monfeli RR, Beeson C (2007) *Infect Disord Drug Targ* 7:213–220
- Vergne AF, Waolz AJ, Miller MJ (2000) *Nat Prod Rep* 17:99–116
- Xu Y, Miller MJ (1998) *J Org Chem* 63:4314–4322
- Roosenberg JM II, Lin YM, Lu Y, Miller MJ (2000) *Curr Med Chem* 7:159–197
- Cronje L, Bornman L (2005) *Int J Tuberc Lung Dis* 9:2–9
- Cronje L, Edmondson N, Eisenach KD, Bornman L (2005) *FEMS Immunol Med Microbiol* 45:103–112
- Fernandes SS, Nunes A, Gomes AR, Castro B, Hider RC, Rangel M, Appelberg R, Gomes MS (2010) *Microbes Infect* 12:287–294
- Bucki R, Pastore JJ, Randhawa P, Vegners R, Weiner DJ, Janmey PA (2004) *Antimicrob Agents Chemother* 48:1526–1533
- Luo M, Fadeev EA, Groves JT (2005) *J Am Chem Soc* 127:1726–1736
- Fadeev EA, Luo M, Groves JT (2004) *J Am Chem Soc* 126:12065–12075
- Xu G, Martinez JS, Groves JT, Butler A (2002) *J Am Chem Soc* 124:13408–13415
- Pahl PMB, Yan XD, Hodges YK, Rosenthal EA, Horwitz MA, Horwitz LD (2000) *J Biol Chem* 275:17821–17826
- Luo M, Fadeev EA, Groves JT (2005) *Nat Chem Biol* 1:149–153
- Tilbrook GS, Hider RC (1998) In: Sigel A, Sigel H (eds) *Metal ions in biological systems*, vol 35. Marcel Dekker, Inc., New York, pp 691–730
- Piyamongkol S, Liu ZD, Hider RC (2001) *Tetrahedron* 57:3479–3486
- Newkome GR, Behera RK, Moorefield CN, Baker GR (1991) *J Org Chem* 56:7162–7167
- Zhou T, Neubert H, Liu DY, Liu ZD, Ma Y, Kong X, Luo W, Mark S, Hider RC (2006) *J Med Chem* 49:4171–4182
- Gran G (1952) *Analyst* 77:661–671
- Gans P, Sabatini A, Vacca A (1996) *Talanta* 43:1739–1753
- Alderighi L, Gans P, Ienco A (1999) *Coord Chem Rev* 184:311–318
- Williams ATR, Winfield SA, Miller JN (1983) *Analyst* 108:1067–1071
- Fiske CH, Subbarow Y (1925) *J Biol Chem* 66:375–400
- Santos NC, Prieto M, Castanho MARB (2003) *BBA Biomembr* 1612:123–135
- Zhou T, Kong X, Liu DY, Liu ZD, Hider RC (2008) *Biomacromolecules* 9:1372–1380
- Liu ZD, Kayyali R, Hider RC, Porter JB, Theobald AE (2002) *J Med Chem* 45:631–639
- Liu ZD, Hider RC (2002) *Coord Chem Rev* 232:151–171
- Burgess J, Rangel M (2008) *Adv Inorg Chem* 60:167–243
- Grazina R, Gano L, Šebestík J, Santos MA (2009) *J Inorg Biochem* 103:262–273
- Mies KA, Gebhardt P, Mollmann U, Crumbliss AL (2008) *J Inorg Biochem* 102:850–861
- Dhungana S, Harrington JM, Gebhardt P, Mollmann U, Crumbliss AL (2007) *Inorg Chem* 46:8362–8371

35. Dhungana S, Ratledge C, Crumbliss AL (2004) *Inorg Chem* 43:6274–6283
36. Dhungana S, Heggemann S, Gebhardt P, Millmann U, Crumbliss AL (2003) *Inorg Chem* 42:42–50
37. Raymond KN, Muller G, Matzanke BF (1984) *Top Curr Chem* 123:49–102
38. Rae TD, Schmidt PJ, Pufahl RA, Culotta VC, O'Halloran TV (1999) *Science* 284:805–808
39. Maret W (2009) *Biomaterials* 22:149–157
40. Glickstein H, Ben El R, Shvartsman M, Cabantchik ZI (2005) *Blood* 106:3242–3250
41. Liu Y, Chen Y, Liu SX, Guan XD, Wada T, Inoue Y (2001) *Org Lett* 3:1657–1660
42. Fasih S, Podinovskaia M, Kong X, Collins HL, Schaible UE, Hider RC (2008) *J Med Chem* 51:4539–4552
43. ChemAxon (2007) Marvin & Marvin version 5.1.4. ChemAxon, Budapest. <http://www.chemaxon.com/products/marvin/>
44. Dhungana S, Miller MJ, Dong L, Ratledge C, Crumbliss AL (2003) *J Am Chem Soc* 125:7654–7663
45. Schwarzenbach G, Schwarzenbach K (1963) *Helv Chim Acta* 46:1390–1400